Catalysis Today 383 (2022) 15–20

Contents lists available at ScienceDirect

Catalysis Today

journal homepage: www.elsevier.com/locate/cattod

Packed-POCS with skin: A novel concept for the intensification of non-adiabatic catalytic processes demonstrated in the case of the Fischer-Tropsch synthesis

Laura Fratalocchi, Gianpiero Groppi, Carlo Giorgio Visconti, Luca Lietti, Enrico Tronconi *

Politecnico di Milano, Dipartimento di Energia, Via La Masa, 34, 20156, Milano, Italy

ARTICLE INFO

This paper is dedicated to Profs. José Antonio Odriozola and Mario Montes on the occasion of their 65th birthday.

Keywords:
Periodic open cellular structure with skin
POCS
Fischer-Tropsch synthesis
Conductive structured catalysts
Heat transfer
Process intensification
3D printing

ABSTRACT

Reaction heat removal/supply is a key issue in the development of intensified compact reactors for non-adiabatic catalytic processes. In this work, using the exothermal Fischer-Tropsch synthesis as a critical case, we show the possibility to boost the heat transfer performances of a packed-POCS (Periodic Open Cellular Structure) reactor by adding an outer metallic thermally connected skin to the conductive cellular internals. To this aim, the performances of a highly active $Co/Pt/Al_2O_3$ catalyst, packed in the form of 300 μm particles into the metallic structure 3D-printed in AlSi7Mg0.6, are assessed at industrially relevant operating conditions and compared with those of the same catalyst particles packed into the same POCS printed without the skin. Outstanding performances (CO conversion in excess of 80 %) are reached with flat axial and radial temperature profiles along the catalytic bed, in line with the excellent temperature control enabled by the conductive POCS. The presence of the skin strongly decreases the overall external temperature difference thanks to the enhanced thermal contact between the reactor wall and the ordered cellular structure, which governs the wall heat transfer. Accordingly, thanks to the presence of the skin, the temperature profile inside the reactor can be controlled much more effectively, thus enabling new operating windows that are not commonly accessible.

1. Introduction

The low-temperature Fischer-Tropsch (LTFT) reaction converts synthesis gas into long straight-chain hydrocarbons that are further processed to maximize the yield into diesel fuels. The LTFT synthesis is carried out at 210−240 °C and 20−30 bar over supported cobalt-based catalysts [1]. Slurry bubble column and multi-tubular fixed bed are the reactor technologies commonly used at the industrial scale [2,3]. For compact applications, multi-tubular fixed bed reactors are preferred due to quasi plug-flow behavior, high catalyst holdup, no need for catalyst separation and easier scalability. However, one of the main issues of this technology is related to the heat removal efficiency, which is critical due to the strong exothermicity of the LTFT ($\Delta H_R^0 \approx -165$ kJ/mol$_{CO}$) [2]. Indeed, temperature management is crucial in order to avoid the presence of hot spots along the catalyst bed, which causes the drop of the process selectivity to long chain hydrocarbons, a faster catalyst deactivation and, in the worst case, the thermal runaway of the reactor [4].

In conventional packed-bed reactors the dominant heat transfer pathway is the flow-dependent forced convection, being the thermal conduction in the solid phase insignificant [2]. In order to improve the heat transfer coefficients and to decrease the heat generation per unit volume [3], in large scale LTFT fixed-bed reactors the heat removal issue is overcome by recycling a fraction of the tail gas, as well as a fraction of produced liquid hydrocarbons. However, this increases the pressure drops and makes the reactor less appropriate for compact/modular biomass to liquid (BTL) or gas to liquid (GTL) technologies, where heat transfer by thermal convection becomes limited by the low flow rate associated with operation in short reaction tubes.

In this perspective, several research groups have focused on the design of reactors with improved thermal management suitable for small-scale Fischer-Tropsch (FT) applications [5–18]. An excellent perspective paper has recently reviewed the developments in the field of structured catalysts and reactors for process intensification, emphasizing the applications to the demanding heat management of LTFT reactors [19]. In fact, structured catalysts and reactors having different configurations, such as microchannels, closed cross flow structures, micro-fibrous entrapped catalysts, honeycomb monoliths, micro-monoliths, open-cell foams and periodic open cellular structures

* Corresponding author.
E-mail address: enrico.tronconi@polimi.it (E. Tronconi).

https://doi.org/10.1016/j.cattod.2020.12.031
Received 28 September 2020; Received in revised form 5 December 2020; Accepted 24 December 2020
Available online 19 January 2021

have been proposed to boost the heat transfer performances of FT packed-bed reactors. It has been demonstrated that heat conduction through the continuous solid matrix of structured reactors or reactor internals can effectively remove the heat generated by the strongly exothermic LTFT and guarantee an excellent temperature control [20].

The optimization of the conductive structured reactors lies in the adoption of "packed structured reactors" [20–22], where the catalyst is randomly packed in the form of pellets in the void of the structured substrates. Indeed, the catalyst load that can be packed in the structure (honeycomb monolith [19], open-cell foam [18,20] or periodic open cell structure, POCS [5]) is much greater than the amount that can be coated on the same structure, providing that the particle size is compatible with the small opening of the structure [5,23], thus boosting the productivity per reactor volume. Noteworthy, pressure drop issues arising from the adoption of small diameter particles can be handled by appropriate design of reactor size (e.g. short tube length) and flow conditions as discussed in [24] with reference to micro packed-bed reactors for the Fischer-Tropsch synthesis.

In this scenario, we have recently demonstrated that thanks to the adoption of a conductive POCS [5] the temperature inside the reactor can be effectively controlled even in the presence of high reaction duty, providing new operating windows that are not accessible using either the conventional packed-bed reactor or the packed-foam technology. Going more into detail, the packed-POCS reactor outperformed the packed-foam reactor [18] in terms of heat transfer granting smaller radial temperature gradients in the catalytic bed, as well as smaller temperature differences at the reactor wall, with larger volumetric thermal power released [5]. The strengths of the packed-POCS reactor configuration with respect to the packed-foam are its regular geometry, which can be optimized to enhance the effective radial thermal conductivity, and the improved contact between the structure and the reactor wall, which governs the limiting wall heat transfer coefficient.

In order to evaluate the possibility to further boost the heat transfer performances of the packed-POCS reactor, in this work we assessed the performances of a POCS with the same geometrical properties (i.e. cell type, cell diameter and void fraction) of the structure already tested in [5] but 3D-printed with a continuous outer metallic skin. This allows to improve the contact between the structure and the reactor wall tube, thus further enhancing the heat transfer properties of the packed-POCS reactor.

2. Experimental

2.1. Packed-POCS reactor

The $Co/Pt/Al_2O_3$ catalyst tested in this work belongs to the same batch of catalyst used in [5]. We recall that it contains 23 wt.% of Co and 0.1 wt.% of Pt supported on γ-Al_2O_3 microspheres (Sasol Puralox) with an average diameter of about 300 μm (for the particle size distribution see the Supplementary Information, Section SI 1). The surface area, the pore volume and the particle density of the catalyst are 59 m^2/g, 0.20 cm^3/g, and 1.32 g/cm^3, respectively. Cobalt, which is initially in its oxide form, can be completely reduced upon H_2-treatment at 400 °C for 17 h. The average size of the metallic Co crystallites dispersed over the Al_2O_3 surface is 9 nm. More details on the catalyst preparation method, as well as on the chemical and physical properties of the $Co/Pt/Al_2O_3$ catalyst, can be found in [25].

The periodic open cellular structure of this study is produced by 3D printing (Renishaw AM250) based on the selective laser melting technology. The starting metal powder is AlSi7Mg0.6 with the following nominal composition: 92.7 wt.% of Al, 6.8 wt.% of Si and 0.5 wt.% of Mg.

As shown in Fig. 1(a, b), the POCS is composed of repeated diamond cells with a diameter (d_{cell}) of 3 mm and a void fraction (ε_{POCS}) of 0.890.

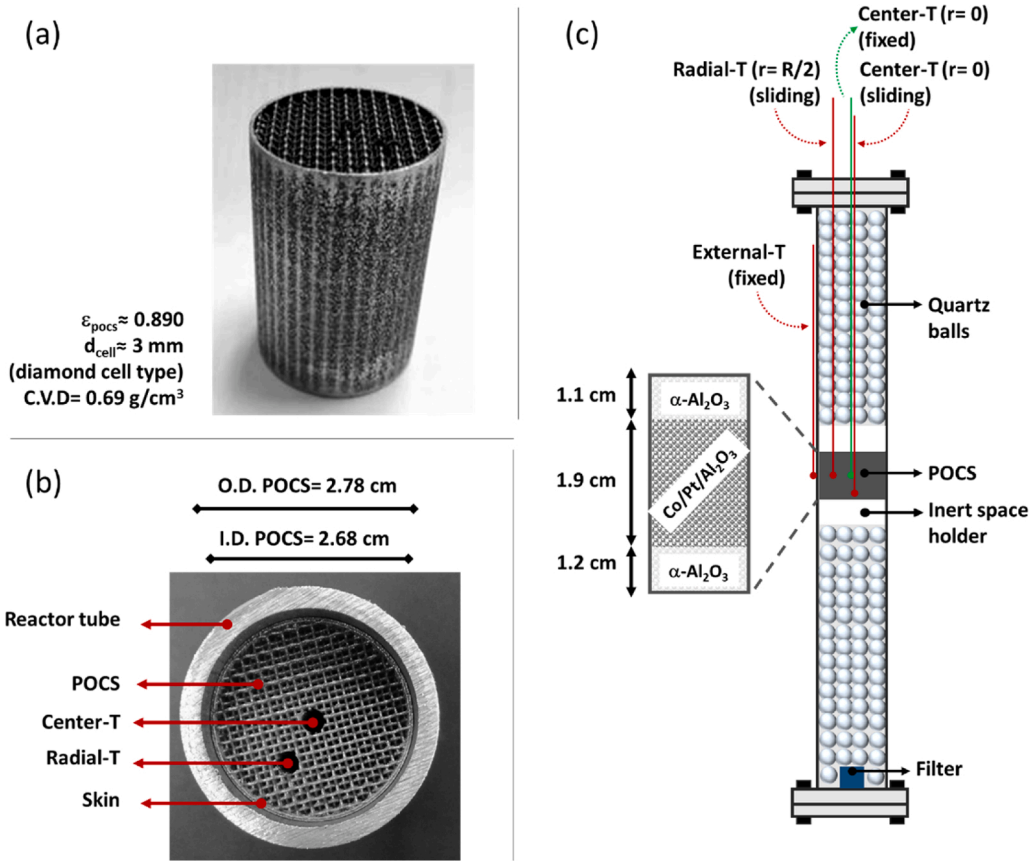

Fig. 1. (a, b) Images of the POCS and (c) schematic diagram of the reactor tube and of the POCS packed with catalyst pellets and α-Al_2O_3.

Cylindrical samples 4.2 cm long have been printed, with an inner diameter of 2.68 cm and an outer 0.5 mm thick metallic skin, thermally connected with the diamond cell internal structure. This results in an outer diameter of the structure of 2.78 cm that matches the inner diameter of the reactor tube so as to reduce the gap resistance.

The two axial through holes of 3.2 mm diameter, clearly visible in Fig. 1(b), are made by electrical discharge machining (EDM). They are located at the centerline of the structure (r = 0) and at half of the radius of the structure (r = R/2) and they are designed for the insertion of stainless steel thermowells (1/8'' O.D.) that accommodate two sliding J-type thermocouples (0.5 mm O.D.). A second J-type thermocouple, which is used to set and control the nominal test temperature, is inserted into the centerline thermowell and located in a fixed position approximately in the middle of the catalyst bed.

The stainless-steel reactor tube 85 cm long is loaded as schematically shown in Fig. 1(c). The POCS is located at about half of the tube in correspondence of the isothermal zone of the oven that covers almost 10 cm in length (ΔT< 0.5 °C). Quartz balls 3 mm in diameter are used as filling material of the remaining volume of the reactor upstream and downstream the catalyst section. The presence of this material also helps the mixing of the reactant gases before the catalyst bed. Quartz fibers, indicated as inert space holder in Fig. 1(c), are used to hold the structure in the proper position and to keep the catalyst particles inside the POCS. Quartz balls and quartz fibers are inert in the FT reaction, as verified experimentally.

Concerning the packing of the structure (Fig. 1(c)), 4.8 g of α-Al_2O_3 pellets are initially poured into the POCS thus forming a 1.2 cm deep layer, followed by a layer containing 7.2 g of Co/Pt/Al_2O_3 catalyst. In order to reach the same catalyst bed length of [5] (1.9 cm), the catalyst is diluted with a very small amount (0.37 g) of α-Al_2O_3 particles with the same diameter (300 μm). Finally, 4.4 g of α-Al_2O_3 pellets are poured into the POCS so to fill the top 1.1 cm of the structure. The resulting average catalyst volumetric density, defined as the ratio of the catalyst mass to the reactor volume occupied by the catalyst bed (10.4 cm^3), is 0.69 g/cm^3.

Notably, the calculated packed-bed porosity (ε_{PB}) is ≈0.38, indicating that the small catalyst pellets (d_{pellet} = 300 μm) uniformly fill the voids of the structure and the presence of the POCS struts has negligible effects on the packing effectiveness. This is related to the high d_{cell}/d_{pellet} ratio [26].

2.2. Catalytic tests

Activity tests are carried out in a single-pass stainless steel fixed-bed reactor (Fig. 1(c)) operating at 25 bar, 190−250 °C (measured at the centerline mid-point of the catalyst bed) and H_2/CO feed ratio of 2.1 mol/mol with 24 mol % inerts (N_2+ Ar), with a gas hourly space velocity (GHSV) of 6410 cm^3(STP)/h/g_{cat}. Further details concerning the experimental set-up can be found elsewhere [27]. Prior to the reaction, the catalyst is activated in situ under a flow of pure H_2 (Sapio, 99.995 mol.%) at 400 °C (heating rate =2 °C/min) and atmospheric pressure for 17 h with a GHSV of 5000 cm^3(STP)/h/g_{cat}.

The full spectrum of products, as well as the unconverted reactants, are measured by on-line and off-line gas-chromatography. More details on the products collection and analysis procedures can be found in [24]. Catalytic activity data have been collected by increasing the reaction temperature from 190 °C to 240 °C with 5 °C steps. A final test has been performed at 250 °C. Each selected temperature has been maintained for more than 48 h, while taking several data points, in order to make sure to collect stationary information at each investigated condition both in terms of CO conversion (X_{CO}, Eq. (1)) and in terms of selectivity to the main reaction products (S_i, Eq. (2)):

$$X_{CO}\ [\%] = \left(1 - \frac{F_{CO}^{out}}{F_{CO}^{in}}\right) \cdot 100 \tag{1}$$

$$S_i\ [\%] = \frac{F_i^{out} \cdot n_i}{\sum_i^{NP}(F_i^{out} \cdot n_i) + F_{CO2}^{out}} \cdot 100 \tag{2}$$

where F_i^{out} is the molar flow of the i^{th} species leaving the reactor, F_{CO}^{in} is the CO molar flow fed to the reactor, n_i is the carbon atom number of the i^{th} species and NP (= 49) is the number of carbon atoms in the heaviest hydrocarbon identified at the product pool. The selectivity to carbon dioxide is calculated as in Eq. (3):

$$S_{CO2}\ [\%] = \frac{F_{CO2}^{out}}{F_{CO}^{in} - F_{CO}^{out}} \cdot 100 \tag{3}$$

Carbon balances, calculated as moles of C contained in the reaction products divided by the moles of CO converted, always closed within ±10 %, being typically within ±5 %.

The volumetric heat duty (Q) is calculated according to Eq. (4):

$$Q\ \left[W/m^3\right] = \frac{-\Delta H_R^0 \cdot F_{CO}^{in} \cdot X_{CO}}{V_{Cat}} \tag{4}$$

where ΔH_R^0 is the standard reaction enthalpy calculated on the basis of the products distribution obtained at different temperatures as reported in [5] and V_{Cat} is the volume of the catalytic section in the adopted POCS sample.

The catalyst stability is verified by comparing the catalyst performances measured at 190 °C at different time on stream (T.o.S.); this operating condition will be referred as "standard". The stability test has been performed after runs at 195 °C (T.o.S. ≈ 217 h), 240 °C (T.o.S. ≈ 913 h) and 250 °C (T.o.S. ≈ 1033 h).

Axial temperature profiles along the catalyst bed are measured at different radial positions by sliding the thermocouples inserted into the thermowells located at the centreline (r = 0) and at the half radius position of the catalyst bed (r = R/2), respectively (Fig. 1c). The axial temperature difference (ΔT_{cat}) is defined as the difference between the maximum and the minimum temperature recorded along the catalyst bed at the centerline. The internal radial temperature difference (ΔT_{rad}) is defined as the difference between the temperature reading at the midpoint of the catalyst bed in centreline (r = 0) and in half radius (r = R/2) position. Another stainless steel thermowell (1/8'' O.D.), protecting a fixed J-type thermocouple (0.5 mm O.D.), is welded to the outer wall of the reactor tube (T_{ext}), in correspondence of the middle of the catalyst bed (Fig. 1c). This enables to evaluate the overall radial temperature difference (ΔT_{ext}), defined as the difference between T_{ext} and the temperature reading at the center of the catalyst bed.

3. Results and discussion

The catalytic performances in the FT measured at different temperatures in the range 190−250 °C, are fully summarized in Section SI 2 of the Supplementary Information and are plotted in terms of CO conversion and selectivities to CH_4 and CO_2 in Fig. 2. CO conversion data in Fig. 2(a) show that the catalyst is already active at temperatures below those commonly used for the FT (<210 °C), indicating the high activity of the adopted Pt-promoted catalyst. In particular, the CO conversion measured at 190 °C is already significant, being near 20 %. The measured CH_4 selectivity is 11.1 %. Upon increasing the temperature, the CO conversion grows up to 85 % at 250 °C where a high CH_4 selectivity of 23.4 % is obtained, in line with data reported in [28].

The selectivity to CO_2 is negligible (i.e. < 2%) up to 220 °C (Fig. 2 (b)). It slightly increases up to 2.5 % at a temperature of 230 °C, while it strongly increases up to 6.0 % and 7.5 %, at 240 °C and 250 °C, respectively. Such an increase, also documented in [25] at high CO conversion levels, is related to the accelerated water gas shift (WGS) kinetics at high water concentrations levels [29]. In turn the higher WGS rate causes an increase in the H_2/CO ratio, responsible for the higher CH_4 selectivity.

Notably, the CO conversion values are similar to those obtained with

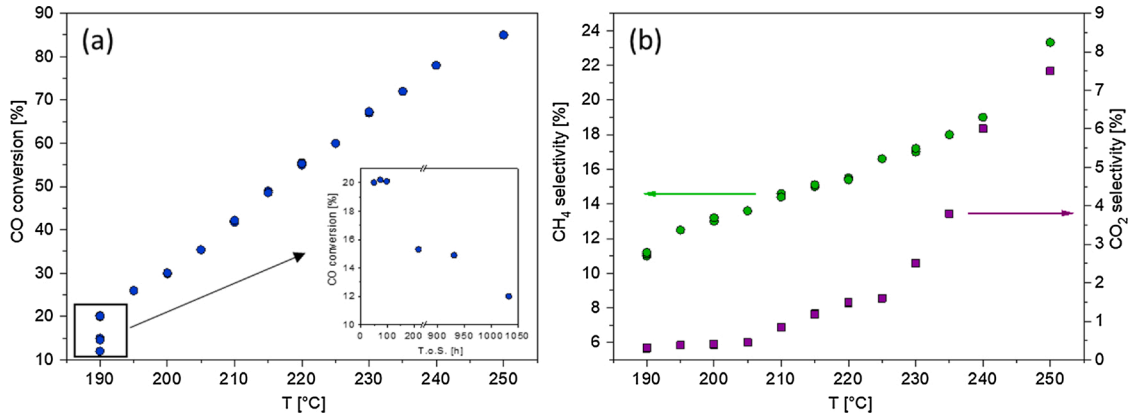

Fig. 2. (a) CO conversion and (b) selectivities to CH_4 (green circle) and CO_2 (violet square) measured at different temperatures in the range 190-250 °C. Inset: CO conversion measured at standard conditions at different T.o.S. (49, 73, 97, 217, 930 1033 h). (o.c.: P=25 bar, H_2/CO^{in}=2.1 mol/mol, GHSV = 6410 cm^3(STP)/h/g_{cat}, in-erts (N_2+Ar)=24 vol.%).

the catalyst packed into the bare POCS up to 195 °C [5], consistently with the fact that the same batch of Co/Pt/Al_2O_3 catalyst is used. However, the activity measured at 200 °C is slightly lower than that reported in [5] with a CO conversion value of 30 % instead of 34 %. This can be attributed to a slight deactivation of the catalyst due to an abrupt shut-down of the experimental rig during heating from 195 °C to 200 °C, that caused the sudden interruption of the syngas supply and the purge of the rig with N_2. In fact, the CO conversions measured by replicating the standard conditions before and after the shut-down (T.o.S. ≈ 97 and 217 h) were respectively 20 % and 15 % (see inset of Fig. 2). After this event, the activity kept stable with T.o.S., as confirmed by the CO conversion of 15 % measured by replicating the standard conditions at 930 h (inset of Fig. 2). Remarkably, this value was obtained after reaching 78 % of CO conversion at 240 °C (T.o.S.≈ 913 h). At variance, the CO conversion at 190 °C dropped from 15 % to 12 % (T.o.S.≈ 1033 h) after reaching 85 % CO conversion at 250 °C (inset of Fig. 2). This suggests that the catalyst is less stable under such severe conditions.

The results obtained in terms of selectivity to short-chain hydrocarbons in the C_2-C_4 range ($S_{C2\text{-}C4}$), long-chain hydrocarbons (S_{C5+}) and olefins and paraffins in the C_2-C_{17} range, are plotted in Fig. 3 at selected temperatures (190, 200, 210, 220 and 230 °C). In line with the increase of the CH_4 selectivity, higher temperatures favor the formation of short chain hydrocarbons, i.e. C_2-C_4 species, with the corresponding decrease of the C_{5+} selectivity (Fig. 3(a)). Indeed, the selectivity to C_2-C_4 hydrocarbons goes from 11 % at 190 °C to 15 % at 230 °C with the opposite trend of the selectivity to C_{5+} that decreases from 76 % at 190 °C to 62 % at 230 °C. These results are consistent with the Anderson-Schulz-Flory (ASF) plots shown in Fig. 4(a). The chain growth probability (α_{C15+}), which is calculated for hydrocarbons with more than 15 carbon atoms [30], follows the same trend of the C_{5+} selectivity, decreasing from 0.887 at 190 °C to 0.850 at 230 °C (Fig. 4(a)).

As shown in Fig. 3(b), the increased selectivity towards the chain termination reactions is linked to an increase of the olefins hydrogenation to paraffins. In this regard, the selectivities to olefins and paraffins in the C_2-C_{17} range at 190 °C are 14 % and 46 % respectively, reaching values of 5% and 60 % when increasing the temperature up to 230 °C. Again, this is also apparent in Fig. 4(b), where the olefin to paraffin ratio is plotted as a function of the carbon number and temperature.

Fig. 5 shows the axial temperature profiles measured in the packed-POCS reactor at different temperatures in the range 190−240 °C. The axial temperature profile at 250 °C was not collected since the catalytic system was extremely unstable and susceptible to any external perturbation. The 1.9 cm zone where the catalyst is present (central area) is highlighted in Fig. 5. Negligible T-differences along the catalyst bed ($\Delta T_{cat} \leq 2$ °C) are observed up to 210 °C. Very limited gradients are also observed at 215 °C (ΔT_{cat}=2.7 °C) and 220 °C (ΔT_{cat}=3.1 °C), although the catalyst reaches 50 % and 55.5 % of CO conversion, respectively. Then, the ΔT_{cat} gradually increases with the CO conversion, going from ΔT_{cat}=4.0 °C at 225 °C (CO conversion of 60 %) up to ΔT_{cat}=6.5 °C at 240 °C (CO conversion of 78 %).

Notably, the presence of an appreciable hot-spot is detectable only when operating the catalyst at 240 °C in correspondence of a volumetric heat duty of the reaction greater than 1500 kW/m^3, thus indicating that the adoption of the highly conductive packed-POCS reactor enables running the LTFT under severe operating conditions with an outstanding temperature control. We recall that the ΔT_{cat} values obtained with this packed-POCS are significantly lower than those obtained when the same reactor tube is packed with the same catalyst, but without the

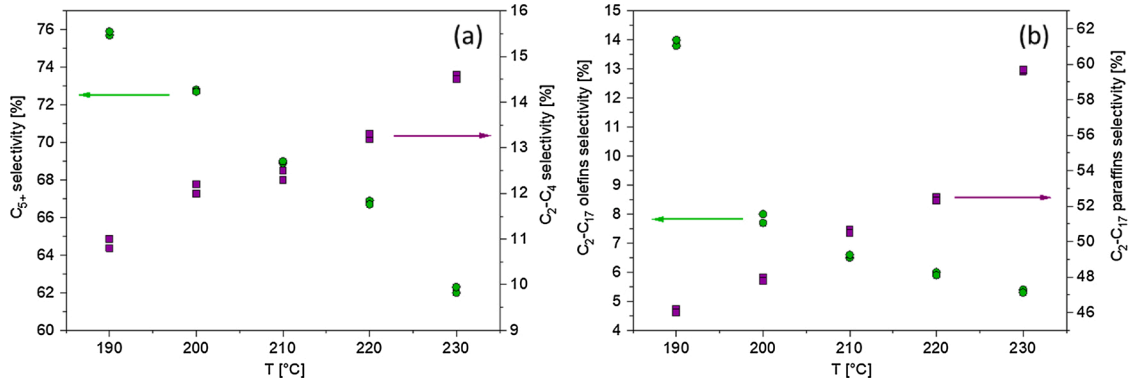

Fig. 3. (a) selectivities to C_{5+} (green circle) and C_2-C_4 (violet square) and (b) selectivities to olefins (green circle) and paraffins (violet square) in the C_2-C_{17} range measured at 190 °C, 200 °C, 210 °C, 220 °C and 230 °C. (o.c.: P=25 bar, H_2/CO^{in}=2.1 mol/mol, GHSV = 6410 cm^3(STP)/h/g_{cat}, inerts (N_2+Ar)=24 vol.%).

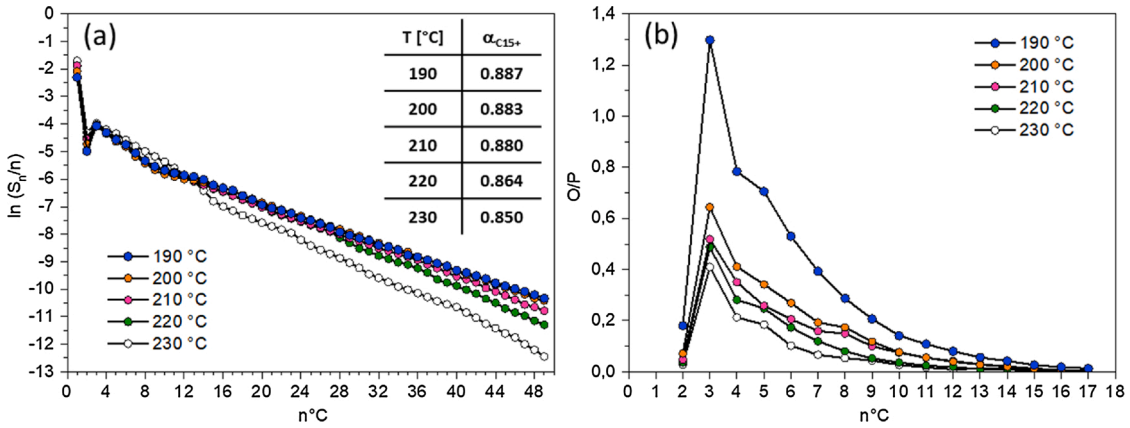

Fig. 4. (a) ASF plots and (b) olefin to paraffin ratio as a function of the carbon number (n°C) measured at 190 °C (blue), 200 °C (orange), 210 °C (pink), 220 °C (green) and 230 °C (white). (o.c.: P=25 bar, H_2/CO^{in}=2.1 mol/mol, GHSV = 6410 cm^3(STP)/h/g_{cat}, inerts (N_2+Ar)=24 vol.%.) (o.c.: P=25 bar, T = 190-250 °C, H_2/CO^{in}=2.1 mol/mol, GHSV = 6410 cm^3(STP)/h/g_{cat}, inerts (N_2+Ar)=24 vol.%.).

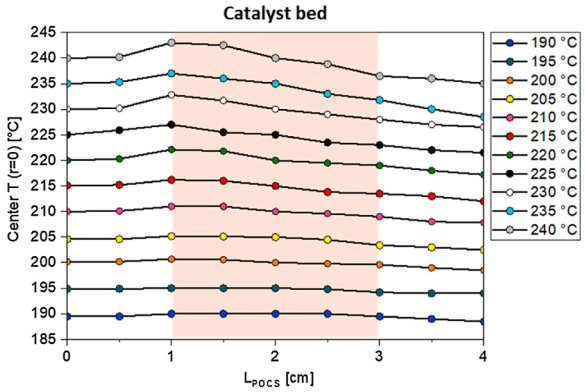

Fig. 5. Axial temperature profiles measured at different temperatures in the range 190-240 °C. The catalyst bed length is highlighted.

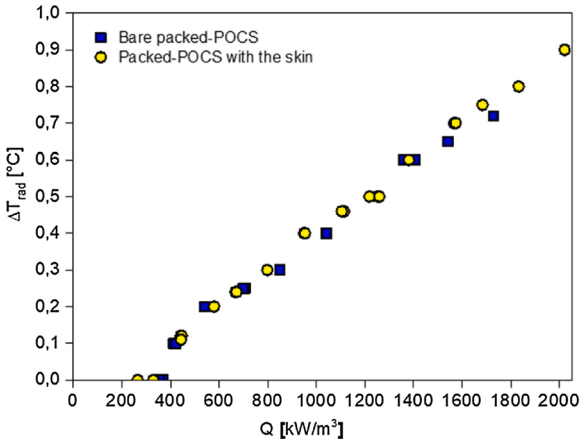

Fig. 6. Radial (ΔT_{rad}) temperature difference as a function of the volumetric heat duty measured during FTS experiments over the bare packed-POCS (blue square) and the packed-POCS with the skin (yellow circle) reactors.

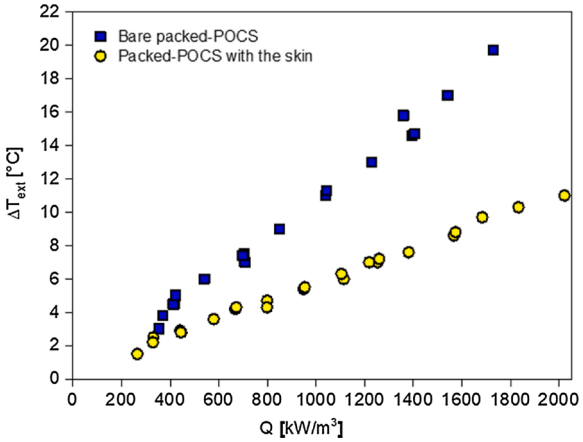

Fig. 7. External (ΔT_{ext}) temperature difference as a function of the volumetric heat duty measured during FTS experiments over the bare packed-POCS (blue square) and the packed-POCS with the skin (yellow circle) reactors.

conductive POCS, even at CO conversions as low as 10 % [18]. Also, we mention here that, when running the same reactor, loaded with the same catalyst and using the same process conditions, we observed a thermal runaway of the reactor above 195 °C, even in the presence of a catalyst bed highly diluted with α-Al_2O_3 [18]. The ΔT_{cat} measured in this work are also slightly lower than those obtained with the bare packed-POCS (no skin) at similar levels of heat release [5], thus indicating an enhancement of the heat transfer by axial conduction due to the presence of the skin.

In order to gain more insight in the effect of the outer metallic skin in the packed-POCS reactor, the heat transfer performances of the structure herein proposed are compared with those of the bare packed-POCS reactor [5] in Figs. 6 and 7. In particular, the radial (ΔT_{rad}) and the external (ΔT_{ext}) temperature differences are plotted for the two configurations against the volumetric heat duty (Eq. (4)) calculated at different reaction temperatures. The ΔH_R^0 values calculated at each reaction temperature are listed in Section SI 2 of the Supplementary Information. It is important to recall that the slope of the data in Fig. 6 reflects the internal effective radial heat conductivity, whereas the slope of the data in Fig. 7 is representative of an overall heat transfer coefficient including also the wall heat transfer resistance.

ΔT_{rad} values less than 1 °C are measured at all the investigated temperatures even when a heat duty in excess of 2000 kW/m^3, corresponding to 85 % CO conversion at 250 °C, is reached (Fig. 6), thus confirming the very high effective internal thermal conductivity of the POCS. Furthermore, it is worth noting that the radial temperature differences of the two packed-POCS configurations (i.e. with and without the skin) are very similar. This is consistent with the fact that the structures share the same geometrical properties (void fraction and cell diameter) and the same node and strut size (node to strut size ratio close to one).

In contrast, major differences are apparent in Fig. 7 where the overall external temperature difference (ΔT_{ext}) is plotted against the volumetric heat duty. Although in the absence of a model-based analysis a rigorous quantitative evaluation of the heat transfer coefficients is not possible due to the complexity of the tested configuration (impact of axial dispersion, role of the top and bottom inert layers), a performance comparison of the two configurations is allowed by their very similar layouts. For this we refer to the slopes of the data in Fig. 7, which can be regarded as roughly representative of overall volumetric heat transfer efficiencies. Such a comparison clearly shows that the packed-POCS with the skin markedly outperforms the bare packed-POCS, being the slope of ΔT_{ext} vs Q about half of that obtained with the POCS printed without the skin, i.e. the overall heat removal efficiency of the POCS with the skin is about twice the one of the bare POCS configuration. Notably, the campaign on the POCS without skin was stopped at 230 °C ($Q = 1730$ kW/m^3) as unstable reactor operation was experienced when trying to push the performances further. In the case of the POCS with skin, a volumetric heat duty in excess of 2000 kW/m^3 is reached at T =250 °C with only a limited ΔT_{ext} of 11 °C. To our knowledge, such a result has never been previously reported in the literature for lab-scale FT reactors [31].

The better overall heat transfer performances of packed-POCS printed with the skin are explained considering that the contact between the reactor wall and the ordered cellular structure, which governs the wall heat transfer coefficient, is enhanced thanks to the presence of the skin.

4. Conclusions

The temperature control is a critical issue for the development of compact fixed bed reactors for strongly exothermic catalytic processes, such as the Fischer-Tropsch synthesis. We have recently shown that the adoption of a highly conductive (Al) random (foam) or periodic open cellular structure (POCS) as reactor internal is an effective solution to enhance the overall heat transfer performances of a packed-bed FT reactor [5]. The POCS showed, indeed, better heat transfer performances than both the packed-bed and the packed-foam reactor configurations. This was attributed to the POCS regular geometry, intensifying both the internal thermal conductivity, and to the improved contact of the ordered structure with the reactor wall, which governs the wall heat transfer coefficient [5]. In this regard, we also showed that the internal heat conduction provided only a minor contribution to the overall heat transfer resistance, which was dominated instead by the wall heat transfer resistance. Accordingly, in order to maximize the contact between the reactor wall tube and the structure, herein we have tested a novel aluminium POCS with the same geometrical properties of the structure already studied in [5], but 3D-printed with an outer metallic skin thermally connected with the internal diamond-structure of the POCS. The collected experimental data confirm that the conductive POCS enables running the LTF Tunder very severe conditions (i.e. high CO conversion and large heat duty) with an outstanding temperature control. Furthermore, the comparison of its thermal behaviour with that of the bare packed-POCS clearly evidences better overall heat transfer performances, as similar volumetric heat duties are reached at significantly lower external temperature differences. Notably, no differences are observed in terms of internal thermal conductivity, in line with the fact that the structures have similar geometrical properties (cell diameter and void fraction). The results herein reported are thus explained considering that the contact between the reactor wall and the ordered cellular structure, which governs the wall heat transfer coefficient, is enhanced thanks to the presence of the skin.

In more general terms, we believe that the concept of conductive packed-POCS with skin may provide an effective design strategy for the intensification of both strongly exothermic and endothermic processes in compact tubular reactors, even in view of retrofitting approaches.

CRediT authorship contribution statement

Laura Fratalocchi: Investigation, Writing - original draft. **Gianpiero Groppi:** Validation, Writing - review & editing. **Carlo Giorgio Visconti:** Data curation, Supervision. **Luca Lietti:** Methodology, Resources. **Enrico Tronconi:** Conceptualization, Funding acquisition.

Declaration of Competing Interest

The authors declare that they have no known competing financial interests or personal relationships that could have appeared to influence the work reported in this paper.

Acknowledgments

This project has received funding from the European Research Council (ERC) under the European Union's Horizon 2020 research and innovation programme (grant agreement No 694910 -'INTENT').

Appendix A. Supplementary data

Supplementary material related to this article can be found, in the online version, at doi:https://doi.org/10.1016/j.cattod.2020.12.031.

References

[1] M.E. Dry, Catal. Today 71 (2002) 227–241.
[2] C.G. Visconti, E. Tronconi, G. Groppi, L. Lietti, M. Iovane, S. Rossini, R. Zennaro, Chem. Eng. J. 171 (2011) 1294–1307.
[3] S.T. Sie, M.M.G. Senden, H.M.H. Van Wechem, Catal. Today 8 (1991) 371–394.
[4] D. Merino, O. Sanz, M. Montes, Chem. Eng. J. 327 (2017) 1033–1042.
[5] L. Fratalocchi, G. Groppi, C.G. Visconti, L. Lietti, E. Tronconi, Chem. Eng. J. 386 (2020) 123988–123997.
[6] D. Merino, O. Sanz, M. Montes, Chem. Eng. J. 327 (2017) 1033–1042.
[7] C.G. Visconti, E. Tronconi, L. Lietti, G. Groppi, P. Forzatti, C. Cristiani, R. Zennaro, S. Rossini, Appl. Catal. A 370 (2009) 93–101.
[8] L.C. Almeida, F.J. Echave, O. Sanz, M.A. Centeno, G. Arzamendi, L.M. Gandìa, E. F. Sousa Aguiar, J.A. Odriozola, M. Montes, Chem. Eng. J. 167 (2011) 536–544.
[9] L.C. Almeida, O. Sanz, D. Merino, G. Arzamendi, L.M. Gandìa, M. Montes, Catal. Today 215 (2013) 103–111.
[10] R. Mystrad, S. Eri, P. Pfeifer, E. Rytter, A. Holmen, Catal. Today 147S (2009) S301–S304.
[11] M. Sheng, H. Yang, D.R. Cahela, W.R. Yantz Jr., C.F. Gonzales, B.J. Tatarchuck, Appl. Catal. A 445–446 (2012) 143–152.
[12] M. Sheng, H. Yang, D.R. Cahela, B.J. Tatarchuck, J. Catal. 281 (2011) 254–262.
[13] M. Lacroix, L. Dreibine, B. de Tymowski, F. Vigneron, D. Edouard, D. Begin, P. Nguyen, C. Pham, S. Savin-Poncet, F. Luck, M.J. Ledoux, C. Pham-Huu, Appl. Catal. A 397 (2011) 62–72.
[14] I. Graf, A.K. Ruhl, B. Kraushaar-Czarnetzki, Chem. Eng. J. 244 (2014) 234–242.
[15] N. Hooshyar, D. Vervloet, F. Kapteijn, P.J. Hamersma, R.F. Mudde, J.R. van Ommen, Chem. Eng. J. 207–208 (2012) 865–870.
[16] B. Kaskes, D. Vervloet, F. Kapteijn, J.R. van Ommen, Chem. Eng. J. 283 (2016) 1465–1483.
[17] H. Becker, R. Güttel, T. Turek, Catal. Sci. Technol. 9 (2019) 2180–2195.
[18] L. Fratalocchi, C.G. Visconti, G. Groppi, L. Lietti, E. Tronconi, Chem. Eng. J. 349 (2018) 829–837.
[19] F. Kapteijn, J. Moulijn, Cat. Today (2020), https://doi.org/10.1016/j.cattod.2020.09.026 in press.
[20] L. Fratalocchi, G. Groppi, C.G. Visconti, L. Lietti, E. Tronconi, React. Chem. Eng. 4 (2019) 1917–1921.
[21] G. Groppi. E. Tronconi, C. G. Visconti, A. Tasso, R. Zennaro, Pat. WO/2015/033266.
[22] C.G. Visconti, G. Groppi, E. Tronconi, Catal. Today 273 (2016) 178–186.
[23] M. Ambrosetti, M. Bracconi, M. Maestri, G. Groppi, E. Tronconi, Chem. Eng. J. 382 (2020), 122801.
[24] C. Knobloch, R. Guttel, T. Turek, Chem. Ing. Technol. 85 (2013) 455–460.
[25] L. Fratalocchi, L. Lietti, C.G. Visconti, N. Fischer, M. Claeys, Catal. Sci. Technol. 9 (2019) 3177–3192.
[26] M. Ambrosetti, G. Groppi, W. Schwieger, E. Tronconi, H. Freund, Chem. Eng. Proc. Proc. Intens. 155 (2020) 108057–108067.
[27] C.G. Visconti, L. Lietti, P. Forzatti, R. Zennaro, Appl. Catal. A 330 (2007) 49–56.
[28] C.L. Tucker, E. van Steen, Catal. Today 342 (2020) 115–123.
[29] L. Fratalocchi, C.G. Visconti, L. Lietti, G. Groppi, E. Tronconi, E. Roccaro, R. Zennaro, Catal. Sci. Technol. 6 (2016) 6431–6440.
[30] Istvan T. Horvath, Encyclopaedia of catalysis, in: Mark E. Day (Ed.), Fischer-Tropsch Synthesis - Industrial, John Wiley & Sons, 2003, pp. 347–403.
[31] A. Egaña, O. Sanz, D. Merino, X. Moriones, M. Montes, Ind. Eng. Chem. Res. 57 (2018) 10187–10197.